Honeycomb-Lattice Mott Insulator on Tantalum Disulphide

Jinwon Lee,[1,2] Kyung-Hwan Jin,[1,3] Andrei Catuneanu,[4] Ara Go,[5,†] Jiwon Jung,[1,2] Choongjae Won,[6,7] Sang-Wook Cheong,[6,7] Jaeyoung Kim,[1] Feng Liu,[3] Hae-Young Kee,[4,8] and Han Woong Yeom[1,2,*]

[1]*Center for Artificial Low Dimensional Electronic Systems, Institute for Basic Science (IBS), Pohang 37673, Republic of Korea*

[2]*Department of Physics, Pohang University of Science and Technology, Pohang 37673, Republic of Korea*

[3]*Department of Materials Science and Engineering, University of Utah, Salt Lake City, Utah 84112, United States*

[4]*Department of Physics, University of Toronto, Ontario M5S 1A7, Canada*

[5]*Center for Theoretical Physics of Complex Systems, Institute for Basic Science (IBS), Daejeon 34126, Republic of Korea*

[6]*Laboratory for Pohang Emergent Materials, Pohang University of Science and Technology, Pohang 37673, Republic of Korea*

[7]*Rutgers Center for Emergent Materials and Department of Physics and Astronomy, Rutgers University, Piscataway, New Jersey 08854, United States*

[8]*Canadian Institute for Advanced Research, CIFAR Program in Quantum Materials, Toronto, Ontario M5G 1M1, Canada*

(Received 20 May 2020; accepted 10 August 2020; published 28 August 2020)

Effects of electron many-body interactions amplify in an electronic system with a narrow bandwidth opening a way to exotic physics. A narrow band in a two-dimensional (2D) honeycomb lattice is particularly intriguing as combined with Dirac bands and topological properties but the material realization of a strongly interacting honeycomb lattice described by the Kane-Mele-Hubbard model has not been identified. Here we report a novel approach to realize a 2D honeycomb-lattice narrow-band system with strongly interacting 5*d* electrons. We engineer a well-known triangular lattice 2D Mott insulator 1*T*-TaS_2 into a honeycomb lattice utilizing an adsorbate superstructure. Potassium (K) adatoms at an optimum coverage deplete one-third of the unpaired *d* electrons and the remaining electrons form a honeycomb lattice with a very small hopping. *Ab initio* calculations show extremely narrow Z_2 topological bands mimicking the Kane-Mele model. Electron spectroscopy detects an order of magnitude bigger charge gap confirming the substantial electron correlation as confirmed by dynamical mean field theory. It could be the first artificial Mott insulator with a finite spin Chern number.

DOI: 10.1103/PhysRevLett.125.096403

Introduction.—An electronic system with an extremely narrow bandwidth has recently attracted huge renewed interests, as it offers a playground to discover exotic quantum phases due to much stronger electron interaction relative to its kinetic energy [1,2]. A narrow band in a two-dimensional (2D) honeycomb lattice is particularly intriguing, as it hosts Dirac electrons with a linear low-energy dispersion as in graphene [3,4], and when the spin-orbit coupling is introduced, a gap opens at Dirac points, leading to a quantum spin Hall state [5]. A sufficiently strong on-site Coulomb repulsion (U) can induce a Mott insulator phase, as described by the Kane-Mele-Hubbard model [6], and various exotic phases have been proposed to emerge such as topologically nontrivial states [7,8], quantum spin liquids [9], charge density waves [7], and superconductivity [10] at or near the half filling, and magnetic Chern insulator at a quarter filling [11]. However, the realization of a 2D honeycomb lattice with strong electron correlation has been challenging since Dirac electrons usually have high kinetic energy. A breakthrough in this challenge was recently achieved by making the Dirac band very flat by twisting two graphene sheets by a magic angle [12,13]. In this system, a correlated insulator and superconductivity [12,13] and more recently a ferromagnetic insulator with a finite Hall conductivity were reported [14–18]. Despite the rapid progress of the research on twisted-bilayer graphene with very small Coulomb energy, the material realization of a Kane-Mele-Hubbard system has been elusive.

In this Letter, we report a unique approach to realize a 2D honeycomb-lattice narrow band system with a strongly interacting 5*d* transition metal. We start from a triangular lattice with a substantial Coulomb interaction and device a way to manipulate the electron hopping into the honeycomb symmetry. The system is based on a well-known 2D Mott insulator 1*T*-TaS_2 and akali metal adsorbates are utilized as the lattice modifier. 1*T*-polytype TaS_2 undergoes a series of spontaneous transitions into various charge-density-wave (CDW) phases [19]. The common unit cell of the CDW phases, known as a David-star cluster, is composed of 13 distorted Ta atoms in a $\sqrt{13} \times \sqrt{13}$ triangular superlattice [Fig. 1(a)]. Each cluster contains 13 Ta 5*d* electrons, 12 of which pair to form insulating CDW bands and to leave one unpaired electron in a

half-filled metallic band. The latter is very flat since the hopping to neighboring David stars is limited by a large distance of ~1.2 nm between them. As a result, a moderate electron correlation U introduces a Mott gap of about 0.2–0.4 eV at low temperature [20–34]. The superconductivity emerging from this insulting state by pressure [35] or chemical doping [36–38] was reported and a quantum spin liquid phase was suggested recently [39–41].

As shown in Fig. 1(b), one can convert a triangular lattice into a honeycomb by eliminating 1/3 of the lattice sites periodically. Figure 1(c) shows a scanning tunneling microscopy (STM) topograph combined with a map of local density of states (LDOS, represented by color) for a $1T$-TaS_2 surface with potassium (K) adatoms of an optimal coverage. At this coverage, K atoms (highly protruded in topograph and blue in the LDOS map) sit selectively at the center of a David-star cluster and form a $(\sqrt{3} \times \sqrt{3})R30°$ superstructure with respect to the CDW lattice [green rhombuses in Fig. 1(b)]. K atoms indeed deplete the unpaired d electron states within a David-star cluster on which it sits as shown in the LDOS map [Fig. 1(c)]. The remaining unpaired electrons in neighboring clusters are little affected by K adatoms and form a honeycomb lattice as illustrated in Figs. 1(b) and 1(c). The Dirac electrons with extremely narrow dispersions and the correlation gap in this system will robustly be justified below.

Methods.—$1T$-TaS_2 single crystal was cleaved in high vacuum to obtain clean surfaces and the K deposition was conducted in ultra high vacuum (1×10^{-10} torr) and at room temperature. STM measurements were performed at 4.4 K in the constant-current mode with a sample bias of −600 meV. A lock-in technique was used in scanning tunneling spectroscopy with a modulation of 1 kHz. The single-particle band structures and their topological properties were investigated within the framework of the density functional theory (DFT) and tight binding calculations [42] and the electron correlation was considered in the dynamical mean field theory (DMFT) calculation [42]. In this work, we only consider a single layer model to describe the surface layer of $1T$-polytype TaS_2. This model is valid for half of the surface layers, which are stacked out-of-phase with the second layer underneath (see more details in the Supplemental Material [42]). The STM data were taken selectively on such layers.

Honeycomb lattice in K-adsorbed $1T$-TaS_2.—The STM image in Fig. 2(a) resolves David-star clusters as medium-contrast protrusions, which is consistent with the previous studies [30,50]. The exceptional features, the prominently bright protrusions, are David-star clusters with one K adatom in each cluster. At the optimized coverage, one third of the CDW unit cells are rather regularly occupied by K atoms. The $\sqrt{3} \times \sqrt{3}$ superstructure of adatoms with respect to the CDW unit cell [the unit cell of the green rhombus in Fig. 2(a)] can be confirmed by the Fourier-transformed STM image of a wide area in Fig. 2(g) (see Fig. 1 in the Supplemental Material [42]). This will be made clear below.

One can notice that David-star clusters with or without K adatoms have totally different electronic states in the scanning tunneling spectra (the normalized dI/dV curves) as shown in Fig. 2(h). Though both spectra show the charge gap, one can clearly see the prominent peaks at −90 and 150 mV on a bare David-star cluster (red data), which are absent in the clusters with K adatoms (green data). Note that the gaps on two different sites have totally different origin. A bare David star has odd number of electrons and its energy gap must originate from a correlated insulating phase as detailed below. The spectral features on a bare David-star cluster are consistent with those of the pristine $1T$-TaS_2, which is established as an Mott insulator (see Fig. 2 in the Supplemental Material [42]). On the other hand, a David star with a K adsorbate has even number of electrons due to the electron donation from K, leading to a simple one-electron gap. The local suppression of the presumed upper and lower Hubbard states (UHS and LHS) by K adatoms is well visualized in the corresponding LDOS maps, or normalized dI/dV maps, of Figs. 2(d) and 2(e), respectively. These LDOS maps further tell us that the

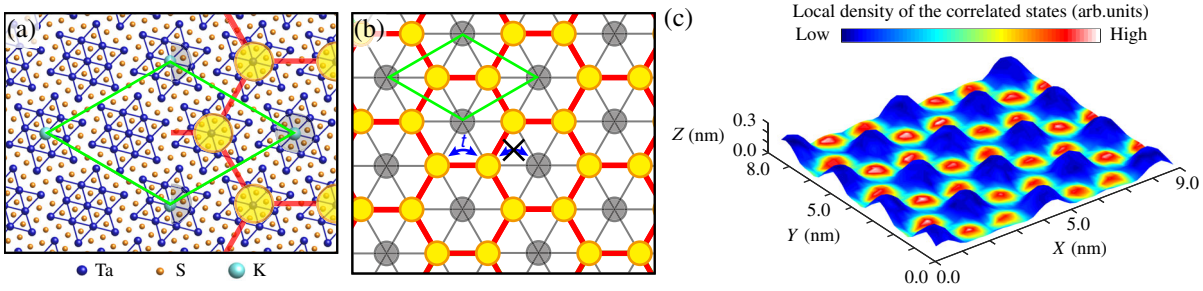

FIG. 1. Honeycomb-lattice correlated phase arising from K adsorption on $1T$-TaS_2. (a) Atomic structure of K-adsorbed $1T$-TaS_2. Blue stars indicate CDW superstructures (David stars) and a green rhombus is a unit cell of K-adsorbed $1T$-TaS_2. (b) A schematic for the honeycomb-lattice correlated phase. Every circle indicates each David star. K-adsorption sites (fully filled states) and bare David stars (half-filled states) are illustrated with gray and yellow color, respectively. Note that a half of (a) is overlaid with the schematic of (b). (c) 3D illustration of the STM topography of K-adsorbed $1T$-TaS_2 (height map) with the local density of the upper Hubbard states (UHS, color map).

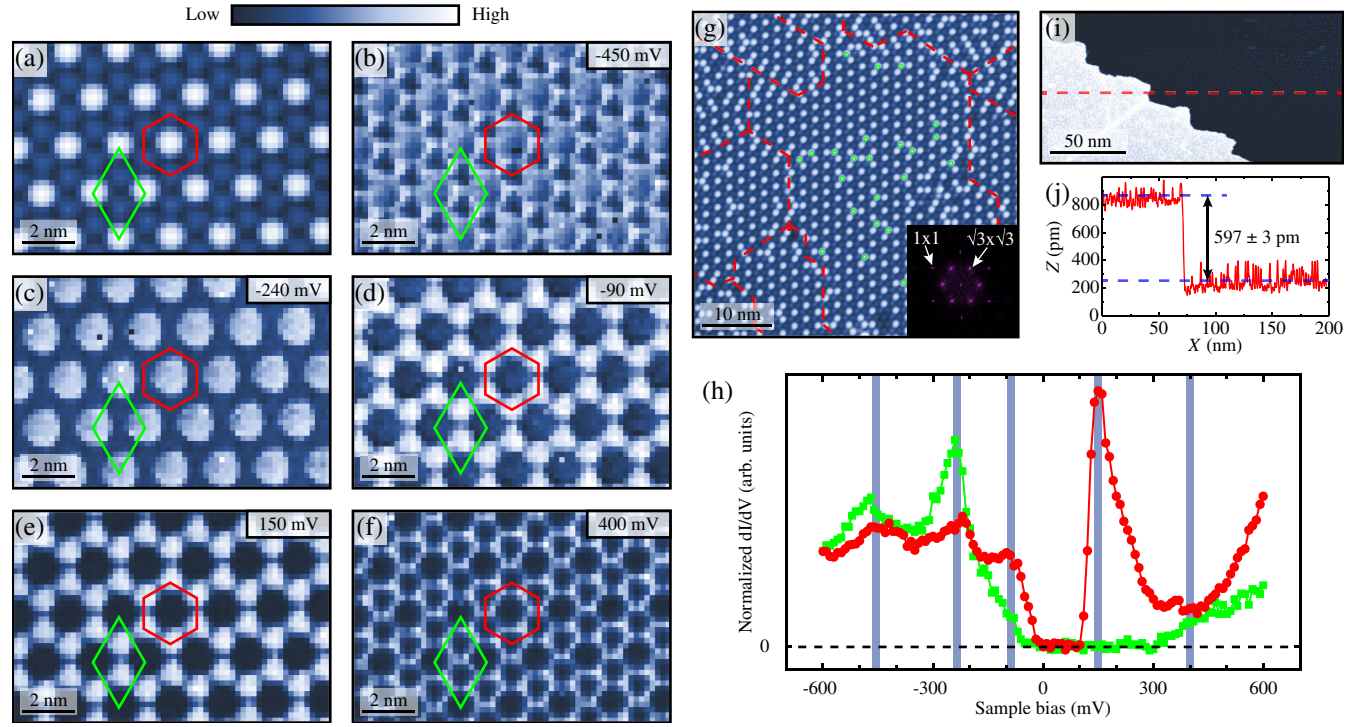

FIG. 2. Local electronic states of K-adsorbed $1T$-TaS_2. (a) STM topographic image of the K-adsorbed $1T$-TaS_2 surface. (b)–(f) Corresponding normalized dI/dV images for $V = -450$, -240, -90, 150, and 400 mV [see vertical bars in (h)]. Note that the features at -90 and 150 mV correspond to correlated Dirac states. (g) A wide-area STM image of $1T$-TaS_2 and its Fourier transform in the inset. 1×1 and $\sqrt{3} \times \sqrt{3}$ stand for the structures with respect to the CDW unit cell. (h) Normalized (dI/dV) spectra at fixed positions. Green and red plots are obtained on the K-adsorption site (green rhombus) and the bare David star (red hexagon), respectively. (i) STM image at a step edge in $1T$-TaS_2 after K deposition. (j) Height (Z) profile along the red dashed line in (i).

correlated states seem to survive in a honeycomb hopping lattice. Note also that the LDOS maps corresponding to CDW bands [Figs. 2(b) and 2(f)] are the same as those in the adsorbate-free area or a pristine sample (see Fig. 2 in the Supplemental Material [42]), telling us that the backbone CDW structure is intact even after the K adsorption.

By passing, we comment further on the adsorption behavior of K atoms. First of all, K atoms are not intercalated but adsorbed on top of the surface S layer as confirmed by the layer spacing (597 pm) [Figs. 2(i) and 2(j)] [51]. DFT calculates the adsorption energy of a K atom on various possible sites within a CDW unit cell (see Note 4, Table I, and Fig. 3 in the Supplemental Material [42]) and finds the center of the David star to be the most energetically favorable. The $4s$ valence electron of a K adatom is almost completely transferred to the substrate to make the adatom ionic [Fig. 3(a)]. It is highly localized on a single David-star cluster, leaving neighboring clusters intact and forming a local dipole. The dipole-dipole interaction explains the repulsion between adatoms to form the ordered superstructure with a domain size up to 30×50 nm^2 [Fig. 2(g)]. Given the short-range repulsion, K atoms adsorb rather randomly avoiding the nearest-neighbor David stars below the optimum coverage (see Fig. 4 in the Supplemental Material [42] for more details of the growth behavior). These calculations agree well with the STM and STS observations.

TABLE I. Parameters of the tight binding Hamiltonian of K-adsorbed $1T$-TaS_2 at the optimal coverage.

Parameter	Value (meV)	Parameter	Value (meV)
t_1	-0.67	t_2	-1.06
t_3	-1.32	t_4	0.26
t_5	0.62	λ_R	0.07
λ_{soc}	0.06		

Electronic structures and topology.—The DFT calculation for $1T$-TaS_2 with K adatoms in a $(\sqrt{3} \times \sqrt{3})R30°$ superstructure predicts two extremely narrow bands at the Fermi energy within the CDW gap as shown in Fig. 3(b). While the two bands are expected from effectively two orphan electrons in a honeycomb supercell with two David-star clusters, the narrow bandwidth with almost linear crossing shown in Figs. 3(c) and 3(d) is notable. The small bandwidth of ~20 meV is due to the d_{z^2} orbital character of those orphan electrons and the huge size of the supercell (see Fig. 5 in the Supplemental Material [42]). The direct hopping integrals between d orbitals in the honeycomb plane are significantly reduced, and the

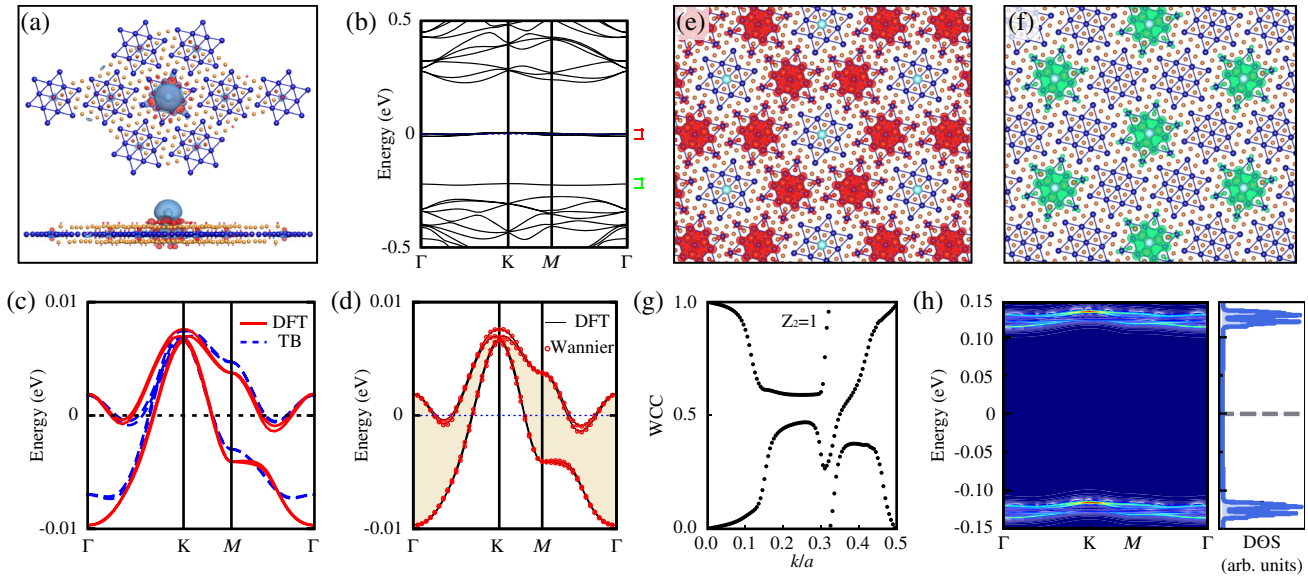

FIG. 3. Electronic band structure of K-adsorbed $1T$-TaS_2. (a) Charge transfer from the K adsorbate. Red and blue colors represent accumulation and depletion of electron, respectively. Note that electron transferred from K adatom is highly localized at the adsorption site. (b) DFT band structure with a paramagnetic constraint. (c),(d) Enlargement of the band structure near the Fermi level with the tight binding (TB) fitting, and the maximally localized Wannier functions fitting, respectively. The colored part in (d) indicates the band gap without any band crossing between the upper and lower Dirac bands, split by the spin-orbit interaction. (e) A spatial distribution of the metallic Dirac bands [marked with red in (b)] and (f) that of a fully occupied band at ~ -0.2 eV [marked with green in (b)]. (g) Evolution of Wannier charge centers by varying the pumping parameter k. The evolution curves have an odd-number crossing with respect to an arbitrary horizontal line. (h) Band structure after considering the electron correlation and the electronic density of states (DOS). The metallic Dirac bands at the Fermi level split with a large charge gap. The extra gaplike feature below each Dirac point is an artifact of the present single-site DMFT calculation.

hopping paths are mainly achieved via p orbitals of S atoms. Given that the inversion symmetry is broken, a finite spin-orbit coupling (SOC) including the Rashba effect splits these bands into four with a tiny gap of ~0.5 meV at K point. Due to time-reversal symmetry, the bands are degenerate at the time-reversal-invariant-momentum points of Γ and M. In addition, a fully occupied band below the Fermi level appears at adsorption sites [marked with a green color in Fig. 3(b)] as originates from the Ta $5d$ level doped with K $4s$ electrons. Its extremely narrow dispersion is due to the strong localization of donated electrons [Fig. 3(a)]. The spatial distributions of two distinct types of electrons are visualized in Figs. 3(e) and 3(f), nicely matching the experimental results [Figs. 2(c)–2(e)].

We investigate the topology of these flat bands by a tight binding model. Indeed, the tight binding model obtained through the Wannier function [52], by projecting the Bloch states from the DFT calculation onto the Ta d_{z^2} orbital (see Note 5 and Figs. 5 and 6 in the Supplemental Material [42]), becomes a characteristic Kane-Mele type Hamiltonian.

$$H = \sum_{i,j,s} t_i c^{\dagger}_{i,s} c_{j,s} + i\lambda_R \sum_{\langle ij \rangle} c^{\dagger}_{i,s} (\vec{\sigma} \times \hat{d}_{ij})^z_{s,s'} c_{j,s'} + i\lambda_{\mathrm{soc}} \sum_{\langle\langle ij \rangle\rangle} c^{\dagger}_{i,s} \nu_{ij} \sigma^z_{s,s'} c_{j,s'}, \quad (1)$$

where $c^{\dagger}_{i,s}$ represents a creation of Wannier state at a cluster i with spin s, and $\vec{\sigma}$ is a Pauli matrix for spin-1/2. $n_{i,s} = c^{\dagger}_{i,s} c_{i,s}$. $\hat{d}_{ij}$ is the unit vector from site j to site i introduced due to the broken inversion symmetry and $\nu_{ij} = \pm 1$ depends on whether the electron hoping from i to j makes a right (+1) or a left (−1) turn. $\langle i, j \rangle$ and $\langle\langle i, j \rangle\rangle$ refer to first and second nearest neighbor (n.n.), respectively, and hopping parameters t_i up to fifth n.n. are used to fit the band dispersion. λ_{soc} and λ_R denote strengths of spin-dependent and Rashba spin-flip SOC, respectively. Tight binding parameters are listed in Table I, which fit the DFT bands well [Fig. 3(c)]. The calculated Wannier charge center [53] indicates clearly an odd number of crossing via the pumping parameter, a hallmark of nontrivial topology of $Z_2 = 1$ [Fig. 3(g)]. The nontrivial order can also be manifested by the presence of helical edge states (see Fig. 7 in the Supplemental Material [42]).

Electron correlation and honeycomb-lattice Mott insulator.—While the DFT results capture the narrow Ta $5d$ bands, its tiny gap is inconsistent with the 200 meV gap observed [see Fig. 2(g) and Fig. 8 in the Supplemental Material [42]). This suggests a crucial role of electron-electron interactions. The electron correlation is considered by performing DMFT calculation using the above Wannier-function tight-binding parameters. As shown in Fig. 3(h), this calculation yields the fully gaped band structure even

with a fairly small Coulomb interaction of 0.25 eV due to the very small hopping integrals or the narrow bands. This unambiguously indicates the strongly correlated, Mott insulating nature of the present system. The occupied and unoccupied bands around −0.1 and 0.1 eV form the LHB and UHB, respectively. The band gap and the narrow LHB band agree well with the above STS results and our angle-resolved photoemission spectroscopy measurements (see Fig. 8 in the Supplemental Material [42]). The topological character of the DFT metallic bands with a direct gap at every momentum points [the colored area in Fig. 3(d)] is preserved here. For example, when the system is half-filled as in the current system, it is a Mott insulator with zero Chern number but with a finite *spin* Chern number, as found in the Kane-Mele model. Increasing U does not change the band topology because the correlation does not break any symmetry as the system remains in the paramagnetic state. This is apparently a Kane-Mele-Hubbard system.

Another possible origin of the insulating phase in our system is a magnetic ordering. Any magnetic orderings in a honeycomb lattice drive the insulating phase due to the time-reversal-symmetry breaking. The system becomes a Chern insulator for $1/4$ and $3/4$ fillings in a ferromagnetic ordering (see Fig. 9 in the Supplemental Material [42]) and a trivial one in an antiferromagnetic case. We considered various magnetic orderings through DFT and spin model calculations (see Note 6 and Figs. 10 and 11 in the Supplemental Material [42]), but the transition temperature is extremely low [$\sim O(\mathrm{mk})$] [42]. Therefore, the experimentally observed charge gap, persisting well above such a low transition temperature, is a strong evidence of the insulating phase without any symmetry breaking, that is the Mott insulator.

We note that the direct experimental confirmation of the topological property itself is missing in the present work. Given that two propagating edge states have different spin Chern numbers, there is no edge states carrying charge in half-filled system. The verification of the topological character, thus, requires doping the system to either $1/4$ or $3/4$ filling, making the system a quantum spin Hall insulator, or removing one of edge states by applying magnetic field to induce a finite Hall conductivity originated from the leftover edge state. The quantized Hall conductivity and STS in a magnetic field in a single layer of K-absorbed $1T$-TaS_2 would be excellent topics of further works together with the tuning of the electron filling to find various exotic phases predicted theoretically. In addition, the robustness of the topological physics against defects in this artificial system is an important issue for future works.

Conclusion.—In this Letter, we create a honeycomb lattice of half-filled d electrons on a $1T$-TaS_2 surface, which is decorated with ordered K adsorbates. The STS data and theoretical considerations indicate unambiguously that the finite-temperature insulating phase of the present system is a honeycomb-lattice Mott insulator described by a supercell Kane-Mele-Hubbard model with a finite spin Chern number for lower and upper Hubbard bands. The lattice manipulation by adsorbate superstructures can widely be exploited in various other 2D materials, in addition to moire superstructures, in order to search and create an exotic electronic system.

This work was supported by the Institute for Basic Science (Grant No. IBS-R014-D1). K.-H. J. and F. L. acknowledge financial support from DOE-BES (Grant No. DE-FG02-04ER46148). K.-H. J. is supported by the Institute for Basic Science (Grant No. IBS-R014-Y1). A. G. thanks financial support from the Institute for Basic Science (Grant No. IBS-R024-D1). A. C. and H.-Y. K. are supported by Natural Sciences and Engineering Research Council of Canada (Grant No. 06089-2016).

Note added.—A very recent theoretical work suggested the realization of a buckled honeycomb lattice in $1T$-$TaSe_2$ through a particular stacking of two layers [54]. This system, however, is not expected to be within the Mott insulator regime due to a substantially, two orders of magnitude, smaller U/t value [54].

*yeom@postech.ac.kr
†Present address: Department of Physics, Chonnam National University, Gwangju 61186, Republic of Korea.

[1] E. J. Bergholtz and Z. Liu, Int. J. Mod. Phys. B **27**, 1330017 (2013).
[2] O. Derzhko, J. Richter, and M. Maksymenko, Int. J. Mod. Phys. B **29**, 1530007 (2015).
[3] K. S. Novoselov, A. K. Geim, S. V. Morozov, D. Jiang, M. I. Katsnelson, I. V. Grigorieva, S. V. Dubonos, and A. A. Firsov, Nature (London) **438**, 197 (2005).
[4] Y. Zhang, Y.-W. Tan, H. L. Stormer, and P. Kim, Nature (London) **438**, 201 (2005).
[5] C. L. Kane and E. J. Mele, Phys. Rev. Lett. **95**, 146802 (2005).
[6] M. Hohenadler, Z. Y. Meng, T. C. Lang, S. Wessel, A. Muramatsu, and F. F. Assaad, Phys. Rev. B **85**, 115132 (2012).
[7] S. Raghu, X.-L. Qi, C. Honerkamp, and S.-C. Zhang, Phys. Rev. Lett. **100**, 156401 (2008).
[8] M. Laubach, J. Reuther, R. Thomale, and S. Rachel, Phys. Rev. B **90**, 165136 (2014).
[9] S.-S. Lee and P. A. Lee, Phys. Rev. Lett. **95**, 036403 (2005).
[10] B. Uchoa and A. H. C. Neto, Phys. Rev. Lett. **98**, 146801 (2007).
[11] A. Mishra and S. Lee, Sci. Rep. **8**, 799 (2018).
[12] Y. Cao, V. Fatemi, A. Demir, S. Fang, S. L. Tomarken, J. Y. Luo, J. D. Sanchez-Yamagishi, K. Watanabe, T. Taniguchi, E. Kaxiras, R. C. Ashoori, and P. Jarillo-Herrero, Nature (London) **556**, 80 (2018).

[13] Y. Cao, V. Fatemi, S. Fang, K. Watanabe, T. Taniguchi, E. Kaxiras, and P. Jarillo-Herrero, Nature (London) **556**, 43 (2018).
[14] J. Kang and O. Vafek, Phys. Rev. Lett. **122**, 246401 (2019).
[15] K. Seo, V. N. Kotov, and B. Uchoa, Phys. Rev. Lett. **122**, 246402 (2019).
[16] A. L. Sharpe, E. J. Fox, A. W. Barnard, J. Finney, K. Watanabe, T. Taniguchi, M. A. Kastner, and D. Goldhaber-Gordon, Science **365**, 605 (2019).
[17] M. Serlin, C. L. Tschirhart, H. Polshyn, Y. Zhang, J. Zhu, K. Watanabe, T. Taniguchi, L. Balents, and A. F. Young, Science **367**, 900 (2020).
[18] C. Repellin, Z. Dong, Y.-H. Zhang, and T. Senthil, Phys. Rev. Lett. **124**, 187601 (2020).
[19] J. A. Wilson, F. J. Di Salvo, and S. Mahajan, Adv. Phys. **24**, 117 (1975).
[20] A. S. Barker, J. A. Ditzenberger, and F. J. DiSalvo, Phys. Rev. B **12**, 2049 (1975).
[21] L. V. Gasparov, K. G. Brown, A. C. Wint, D. B. Tanner, H. Berger, G. Margaritondo, R. Gaál, and L. Forró, Phys. Rev. B **66**, 094301 (2002).
[22] F. Zwick, H. Berger, I. Vobornik, G. Margaritondo, L. Forró, C. Beeli, M. Onellion, G. Panaccione, A. Taleb-Ibrahimi, and M. Grioni, Phys. Rev. Lett. **81**, 1058 (1998).
[23] F. Clerc, C. Battaglia, M. Bovet, L. Despont, C. Monney, H. Cercellier, M. G. Garnier, P. Aebi, H. Berger, and L. Forró, Phys. Rev. B **74**, 155114 (2006).
[24] L. Perfetti, P. A. Loukakos, M. Lisowski, U. Bovensiepen, M. Wolf, H. Berger, S. Biermann, and A. Georges, New J. Phys. **10**, 053019 (2008).
[25] H. Sato, M. Arita, Y. Utsumi, Y. Mukaegawa, M. Sasaki, A. Ohnishi, M. Kitaura, H. Namatame, and M. Taniguchi, Phys. Rev. B **89**, 155137 (2014).
[26] T. Ritschel, J. Trinckauf, K. Koepernik, B. Büchner, M. v. Zimmermann, H. Berger, Y. I. Joe, P. Abbamonte, and J. Geck, Nat. Phys. **11**, 328 (2015).
[27] I. Lutsyk, M. Rogala, P. Dabrowski, P. Krukowski, P. J. Kowalczyk, A. Busiakiewicz, D. A. Kowalczyk, E. Lacinska, J. Binder, N. Olszowska, M. Kopciuszynski, K. Szalowski, M. Gmitra, R. Stepniewski, M. Jalochowski, J. J. Kolodziej, A. Wysmolek, and Z. Klusek, Phys. Rev. B **98**, 195425 (2018).
[28] J.-J. Kim, W. Yamaguchi, T. Hasegawa, and K. Kitazawa, Phys. Rev. Lett. **73**, 2103 (1994).
[29] J.-J. Kim, I. Ekvall, and H. Olin, Phys. Rev. B **54**, 2244 (1996).
[30] D. Cho, Y.-H. Cho, S.-W. Cheong, K.-S. Kim, and H. W. Yeom, Phys. Rev. B **92**, 085132 (2015).
[31] D. Cho, S. Cheon, K.-S. Kim, S.-H. Lee, Y.-H. Cho, S.-W. Cheong, and H. W. Yeom, Nat. Commun. **7**, 10453 (2016).
[32] L. Ma, C. Ye, Y. Yu, X. F. Lu, X. Niu, S. Kim, D. Feng, D. Tománek, Y.-W. Son, X. H. Chen, and Y. Zhang, Nat. Commun. **7**, 10956 (2016).
[33] D. Cho, G. Gye, J. Lee, S.-H. Lee, L. Wang, S.-W. Cheong, and H. W. Yeom, Nat. Commun. **8**, 392 (2017).
[34] C. J. Butler, M. Yoshida, T. Hanaguri, and Y. Iwasa, Nat. Commun. **11**, 2477 (2020).
[35] B. Sipos, A. F. Kusmartseva, A. Akrap, H. Berger, L. Forró, and E. Tutiš, Nat. Mater. **7**, 960 (2008).
[36] P. Xu, J. O. Piatek, P.-H. Lin, B. Sipos, H. Berger, L. Forró, H. M. Rønnow, and M. Grioni, Phys. Rev. B **81**, 172503 (2010).
[37] L. J. Li, W. J. Lu, X. D. Zhu, Z. Qu, and Y. P. Sun, Europhys. Lett. **97**, 67005 (2012).
[38] Y. Liu, R. Ang, W. J. Lu, W. H. Song, L. J. Li, and Y. P. Sun, Appl. Phys. Lett. **102**, 192602 (2013).
[39] K. T. Law and P. A. Lee, Proc. Natl. Acad. Sci. U.S.A. **114**, 6996 (2017).
[40] A. Ribak, I. Silber, C. Baines, K. Chashka, Z. Salman, Y. Dagan, and A. Kanigel, Phys. Rev. B **96**, 195131 (2017).
[41] M. Klanjšek, A. Zorko, R. Žitko, J. Mravlje, Z. Jagličić, P. K. Biswas, P. Prelovšek, D. Mihailovic, and D. Arčon, Nat. Phys. **13**, 1130 (2017).
[42] See the Supplemental Material at http://link.aps.org/supplemental/10.1103/PhysRevLett.125.096403 for the details, which includes Refs. [34,43–49].
[43] G. Kresse and J. Furthmüller, Phys. Rev. B **54**, 11169 (1996).
[44] J. P. Perdew, K. Burke, and M. Ernzerhof, Phys. Rev. Lett. **77**, 3865 (1996).
[45] A. Georges, G. Kotliar, W. Krauth, and M. J. Rozenberg, Rev. Mod. Phys. **68**, 13 (1996).
[46] M. Caffarel and W. Krauth, Phys. Rev. Lett. **72**, 1545 (1994).
[47] C. H. Kim, S. Baidya, H. Cho, V. V. Gapontsev, S. V. Streltsov, D. I. Khomskii, J.-G. Park, A. Go, and H. Jin, Phys. Rev. B **100**, 161104(R) (2019).
[48] J. Oitmaa and R. R. P. Singh, Phys. Rev. B **84**, 094424 (2011).
[49] S.-S. Gong, D. N. Sheng, O. I. Motrunich, and M. P. A. Fisher, Phys. Rev. B **88**, 165138 (2013).
[50] B. Giambattista, C. G. Slough, W. W. McNairy, and R. V. Coleman, Phys. Rev. B **41**, 10082 (1990).
[51] P. Schmidt, B. Murphy, J. Kröger, H. Jensen, and R. Berndt, Phys. Rev. B **74**, 193407 (2006).
[52] A. A. Mostofi, J. R. Yates, G. Pizzi, Y.-S. Lee, I. Souza, D. Vanderbilt, and N. Marzari, Comput. Phys. Commun. **185**, 2309 (2014).
[53] A. A. Soluyanov and D. Vanderbilt, Phys. Rev. B **83**, 235401 (2011).
[54] J. M. Pizarro, S. Adler, K. Zantout, T. Mertz, P. Barone, R. Valentí, G. Sangiovanni, and T. O. Wehling, arXiv:2001.04102.